The International Journal of Advanced Manufacturing Technology (2018) 98:603–615
https://doi.org/10.1007/s00170-018-2265-6

ORIGINAL ARTICLE

Investigation on formation mechanism of surface texture and modeling of surface roughness with internal gear power honing

Jiang Han[1] · Guozheng Zhang[1]

Received: 27 November 2017 / Accepted: 31 May 2018 / Published online: 14 June 2018

Abstract

In order to understand the formation mechanism of surface arc texture of internal gear power honing, the contact line equation of tooth surface is derived with homogeneous coordinate transformation method, which is based on the involute helical tooth surface equation of honed workpiece gear as well as the meshing principle of space surface. Then the influence of shaft angle Σ on the formation of surface arc texture of workpiece is analyzed. The results of imager and three-dimensional (3D) profilometer are in accordance with the theoretical derivation. In order to analyze the influence of the power honing process parameters on the surface roughness, a central composite surface design method based on response surface methodology (RSM) is proposed in a range of process parameters. Based on this, a regression model of surface roughness for the honed workpiece gear is established. Meanwhile, the influence of power honing process parameters on the surface roughness of honed workpiece gear is analyzed. The process parameters are the honing wheel speed n_H, Z feed f_Z, and X feed f_X. The three-dimensional profilometer is utilized to analyze the roughness value with a set of process parameters, based on which the accuracy and reliability of the model can be verified. The results show that the surface arc texture is suitable for producing dense textures when the shaft angle Σ is within 5° to 10°. According to the analysis, n_H has the greatest influence on the surface roughness of the honed workpiece gear. The effects of f_Z and f_X are almost the same when $R_a \geq 0.4$ μm, and while $R_a \leq 0.3$ μm, the effect of f_Z is slightly higher than that of f_X, R_a is the regression value obtained after the honing process. Based on the mention above, the surface quality of the honed workpiece gear can be predicted and controlled before honing.

Keywords Internal gear power honing · Surface arc texture · Formation mechanism · Regression model of roughness · Response surface methodology (RSM)

Nomenclature

Σ	Shaft angle
R_a	Surface roughness
n_H	Honing wheel speed
f_Z	Z feed
f_X	X feed
r_b	Radius of base cylinder
σ_0	Starting angle
u	Generating angle
θ	Rotation angle
p	Pitch
S_1	Workpiece gear coordinate system
S_2	Internal gear honing wheel coordinate system
a	Distance of the two wheels
ω_1,ω_W	Rotation speeds of workpiece gear
ω_2,ω_H	Rotation speeds of internal gear honing wheel
ϕ_1	Rotation angle of workpiece gear
r_H	Position vectors of internal gear honing wheel
r_W	Position vectors of workpiece gear
v_{WH}^M	Point M is the relative velocity in the coordinate system S (O-x, y, z)
v_W	Velocity of workpiece gear
v_H	Velocity of internal gear honing wheel
i_{12}	Transmission ratio
n	Unit normal vector
B_1	Tooth width
Y	Prediction value of surface roughness
ε	Error term

✉ Guozheng Zhang
zgzaust@163.com

[1] CIMS institute, Hefei University of Technology, Hefei City, Anhui Province, China

1 Introduction

Finishing process is a primary approach to eliminate the heat treatment-induced deformation and improve the tooth surface accuracy and quality [1–3]. The generating method is often applied to the precision manufacturing of high-grade gear-box for automobile, especially the application of internal gear power honing process [4–5].With the development of numerical controlled (NC) electronic gear-box, traditional free honing process is replaced by NC power honing process, especially the internal gear power honing process. It can save the cost of high-precision gear manufacturing and improve the precision of tooth surface as well as manufacturing, since it is considered as the last finishing process [6–8]. Amini. N and Westberg. H [9] proved that the internal gear power honing process can effectively reduce the vibration and noise generated by the transmission of honed workpiece gear, since the surface of internal gear power honing is the arc texture while gear grinding is the periodic and circular texture which cannot suppress the noise of gear transmission.

Although the arc texture is verified by simulating and experimenting, there is lack of theoretical analysis, for example, reports on the formation mechanism of tooth surface arc texture from the shaft angle are few. Most of the researchers who are engaged in the analysis of the tooth surface geometry and gear manufacturing have carried out the analysis of surface texture from instrumental detection, numerical simulation, experimental analysis, and abrasive cutting. For example, JOLIVET et al. [10–11] utilized the interferometer to detect the tooth surface after honing. However, the tooth surface texture cannot be fully expressed and the accuracy evaluation of tooth surface with 3D shape needs to be improved since the tooth surface area is too small. DENKENA et al. [12] applied numerical simulation technology to analyze the tooth surface texture, and the simulation results are reliable. Through the establishment of the surface topography of the grinding wheel and the interference of the workpiece surface cut by single or multiple abrasive particles, the relevant scholars evaluate the surface geometric texture of the workpiece by computational simulation technology. For example, Chakrabarti et al. [13] proposed the prediction of the surface roughness with uniform distribution of abrasive grains. However the initial condition of grinding wheel is not in a uniformly distributed state, and it approximates the Gaussian distribution which can be modified to uniform distribution. Therefore, the method that evaluates the surface of grinding wheel and then analyzes the texture of workpiece surface according to the abrasive cutting needs to be improved. Nguyen et al. [14] measured the topography of actual grinding wheel and then establishes the virtual simulation model. Hecker [15] and Stepien [16] considered that abrasive particles should randomly distribute on the surface of the grinding wheel to predict surface roughness. According to the research results of Thyssen [17], Karpuschewski [18] utilized the numerical simulation method to simulate the surface topographies of straight tooth generating grinding, helical tooth generating grinding, and gear honing, the simulation results show that there are two directions of velocity between the honing wheel and the honed workpiece gear. The two directions are tooth direction slip and the tooth profile slip. Then the abrasive grains on the honing wheel are cutting on the tooth surface of the honed workpiece gear, which forms the arc texture. The above research can only demonstrate that honing can produce arc texture. However, the formation mechanism of the arc texture of internal gear power honing is not theoretically analyzed in terms of meshing transmission in space interleaving. In order to further understand the formation mechanism, the equation of tooth surface is derived with homogeneous coordinate transformation method, which is based on the involute helical tooth surface equation of honed workpiece gear, the meshing principle of space surface, and contact line equation of tooth surface. Meanwhile, the effect of shaft angle Σ on the formation of surface arc texture of honed workpiece gear is also analyzed. The tooth surface is observed and analyzed by 3D profilometer after power honing. Based on this, the formation mechanism of arc texture is verified.

Roughness is an essential characteristic of surface texture and its value is an important parameter to measure the mechanical processing level of workpiece surface. Roughness has a crucial effect on the fatigue resistance and surface friction properties of the components, assembly motion stability, wear resistance, and service life [19–20]. The Ra value of ISO4287 standard is used to evaluate the surface roughness. In this paper, the Ra value is used to predict the roughness of tooth surface. As for the prediction of roughness model, most of the research adopt the roughness peak that assumes accordance with the Gaussian distribution to evaluate the simulation [21–22]. However, it has a certain degree of deviation from the actual surface roughness. As for the regression modeling methods of roughness, Fuzzy Nets (FN), Artificial Neural Network (ANN), and support vector machine are used in milling surface roughness [23–25]. In order to ensure the accuracy of the model, these methods either require large number of samples, large test volume, and complex modeling, or it is difficult to determine the nonlinear optimal parameters. Sandro et al. [26] utilized the RSM to establish the predicted models of the total tooth profile deviation, the total helix deviation, and the total gear pitch deviation of the internal gear power honing. These models are optimized by the particle swarm optimization. On the basis of the technical parameters provided by the internal gear power honing manufacturers, the RSM can be used to predict the surface roughness accurately. Considering the fuzziness of the influence degree of f_Z and f_X on the roughness in the response surface, the influence degree

of these two process parameters on roughness can be further clarified by constructing iso-surface analysis of different Ra value. Considering the accuracy of the measuring equipment or the difference of sampling scales, the detected roughness may bias [27]. The 3D profilometer is utilized to analyze the roughness value with a set of process parameters, based on which the accuracy and reliability of the regression model can be verified.

2 Establishment of the contact line equation of tooth surface

2.1 Tooth surface equation of workpiece

According to the formation principle of involute tooth surface, the tooth surface of workpiece is an involute helicoid, which is shown in Fig. 1.

As can be seen from Fig. 1, S (O-x, y, z) is the inherent coordinate system of the workpiece gear, r_b is the radius of base cylinder, e is the starting point of involute on the end of the basic cylinder, and σ_0 is the starting angle. M is an arbitrary point on the involute ef, which is tangent to the basic circle in point a. $\angle eOa = u$ is the generating angle of point M, it is a variable parameter. The involute ef takes helical motion with equal pitch around the Z axis. θ is the rotation angle between point M and M' while $p\theta$ is the moving distance on Z axis of the basic cylinder. The formed surface is an involute helicoid when ef arrives at point B. The equation of the involute helicoid is expressed as:

$$\begin{cases} x = r_b\cos(\sigma_0 + u + \theta) + r_b u\sin(\sigma_0 + u + \theta) \\ y = r_b\sin(\sigma_0 + u + \theta) - r_b u\cos(\sigma_0 + u + \theta) \\ z = p\theta \end{cases} \quad (1)$$

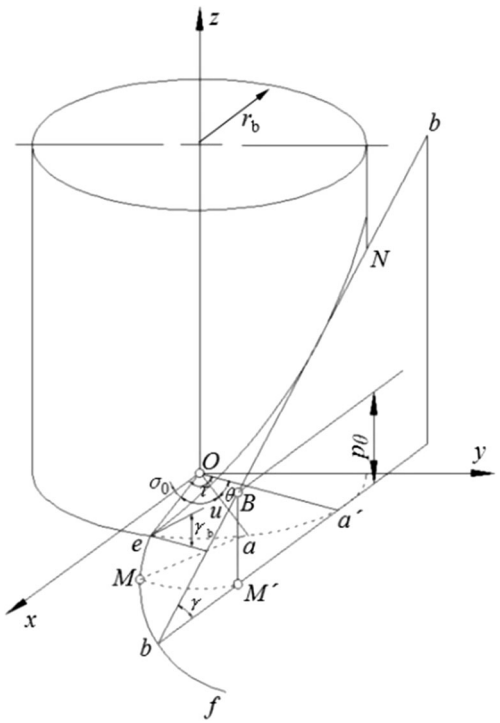

Fig. 1 The formation principle of involute helicoid

2.2 The contact line equation of tooth surface

According to the meshing principle and the conjugate theory of tooth surface, the contact line equation of tooth surface is established. The conjugate surface between internal gear honing wheel and workpiece gear remains in continuous contact in the transmission process. The tooth surface equation of the conjugate gear is derived by a known tooth surface equation, which is based on the envelope principle of gear meshing. Then the contact line equation of tooth surface can be established. The spatial coordinate relationship between internal gear honing wheel and workpiece gear is shown in Fig. 2.

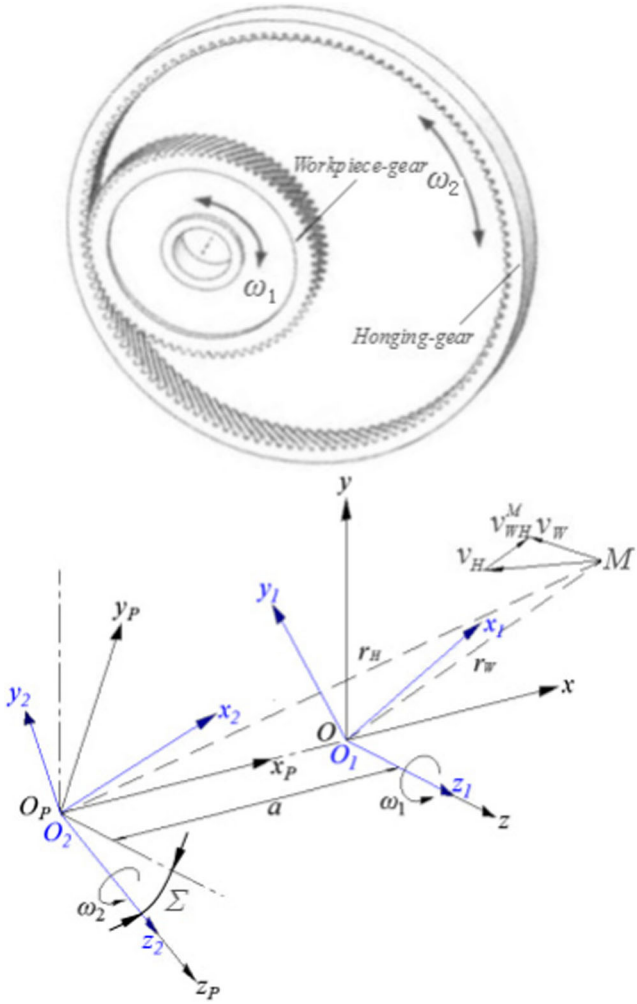

Fig. 2 Spatial coordinate system of internal gear honing wheel and workpiece gear

In Fig. 2, the coordinate system $S_1(O_1\text{-}x_1, y_1, z_1)$ coincides with the fixed coordinate system $S(O\text{-}x, y, z)$ of the workpiece gear and the coordinate system $S_2(O_2\text{-}x_2, y_2, z_2)$ coincides with the fixed coordinate system $S_p(O_p\text{-}x_p, y_p, z_p)$of the internal gear honing wheel. In the internal gear honing process, the two wheels rotate around the z_1 and z_2 axes and the rotation speeds are $\boldsymbol{\omega}_1$ and $\boldsymbol{\omega}_2$, respectively. φ_1 is the rotation angle that the workpiece gear rotates around the self-rotation axis, and only the rotation axes z_1 and z_2 are consistent with z and z_p in their fixed coordinate systems. a is the distance of the two wheels, that is, the distance of the two axes. Σ is the shaft angle of the two axes, it is supposed to be between ω_1 and ω_2. Subscript W (Workpiece-gear) represents the relevant parameters of the workpiece gear, and subscript H (Honging-gear) represents the parameters of the internal gear honing wheel. r_W and r_H represent the position vectors of arbitrary meshing point M to their respective coordinate origin on the instantaneous contact line, so v_{WH}^M of point M is the relative velocity in the coordinate system $S(O\text{-}x, y, z)$. By means of homogeneous coordinate transformation method, the position vectors of arbitrary meshing point on the contact line can be derived, as well as the angular speeds of workpiece gear and internal gear honing wheel in the coordinate system $S(O\text{-}x, y, z)$. The vector equations are expressed as:

$$r_W = \begin{pmatrix} x \\ y \\ z \end{pmatrix} = T_{O1} r_{W1} = \begin{pmatrix} x_1\cos\phi_1 - y_1\sin\phi_1 \\ x_1\sin\phi_1 + y_1\cos\phi_1 \\ z_1 \end{pmatrix} \tag{2}$$

$$r_H = r_W + \begin{pmatrix} a \\ 0 \\ 0 \end{pmatrix} = \begin{pmatrix} x + a \\ 0 \\ 0 \end{pmatrix} \tag{3}$$

$$\omega_W = \omega_1 \begin{pmatrix} 0 \\ 0 \\ 1 \end{pmatrix} \tag{4}$$

$$\omega_H = \begin{pmatrix} 1 & 0 & 0 \\ 0 & \cos\Sigma & -\sin\Sigma \\ 0 & \sin\Sigma & \cos\Sigma \end{pmatrix} \begin{pmatrix} 0 \\ 0 \\ \omega_1/i_{12} \end{pmatrix} = \omega_1/i_{12} \begin{pmatrix} 0 \\ -\sin\Sigma \\ \cos\Sigma \end{pmatrix} \tag{5}$$

v_{WH}^M is expressed as:

$$v_{WH}^M = v_W - v_H = \omega_W \times r_W - \omega_H \times r_H \tag{6}$$

The vector expression of v_{WH}^M in coordinate system $S(O\text{-}x, y, z)$ can be obtained by Eqs. (2)–(6) and it is expressed as:

$$v_{WH}^M = \omega_1 \begin{pmatrix} -y + (y\cos\Sigma + z\sin\Sigma)/i_{12} \\ x - (x + a)\cos\Sigma/i_{12} \\ -(x + a)\sin\Sigma/i_{12} \end{pmatrix} \tag{7}$$

According to the meshing geometry theory of the gear, whether the conjugate tooth surfaces are line contact or point contact, the meshing equation of the conjugate point M is expressed as [28]:

$$v_{WH}^M \cdot n = 0 \tag{8}$$

The normal vector of arbitrary point on the contact line of workpiece surface in coordinate system $S(O\text{-}x, y, z)$ can be expressed as:

$$n = \begin{pmatrix} n_x \\ n_y \\ n_z \end{pmatrix} = \begin{pmatrix} cos\phi_1 & -sin\phi_1 & 0 \\ sin\phi_1 & cos\phi_1 & 0 \\ 0 & 0 & 1 \end{pmatrix} \begin{pmatrix} n_{1x} \\ n_{1y} \\ n_{1z} \end{pmatrix} = \begin{pmatrix} n_{1x}cos\phi_1 - n_{1y}sin\phi_1 \\ n_{1x}sin\phi_1 + n_{1y}cos\phi_1 \\ n_{1z} \end{pmatrix} \tag{9}$$

According to Eqs. (8) and (9), the meshing equation of the tooth surface in coordinate system $S(O\text{-}x, y, z)$ is derived and it is expressed as:

$$n_x\omega_1[-y + (y\cos\Sigma + z\sin\Sigma)/i_{12}] + n_y\omega_1[x - (x + a)\cos\Sigma/i_{12}] - n_z\omega_1[(x + a)\sin\Sigma/i_{12}] = 0 \tag{10}$$

where i_{12} is the transmission ratio of the two gears. When the arbitrary point M on involute helicoid rotates a certain angle and reaches point M', the vector value can be expressed by $S_1(x_1, y_1, z_1)$.

$$r_{W1} = \begin{pmatrix} r_{b1}\cos(\sigma_0 + u + \theta) + r_{b1}\mu\sin(\sigma_0 + u + \theta) \\ r_{b1}\sin(\sigma_0 + u + \theta) - r_{b1}\mu\cos(\sigma_0 + u + \theta) \\ p\theta \end{pmatrix} \tag{11}$$

The conjugate contact equation of tooth surface under $S_1(x_1, y_1, z_1)$ can also be deduced by homogeneous coordinate transformation method.

$$\begin{aligned} f(\theta, u, \phi_1) = {} & \left[\left(\theta p^2 - u r_{b1}^2\right)\sin\Sigma\sin(\sigma_0 + \theta + u + \phi_1)\right. \\ & + \left(ap\cos\Sigma - r_{b1}^2\sin\Sigma\right)\cos(\sigma_0 + \theta + u + \phi_1) \\ & \left. + (p\cos\Sigma - a\sin\Sigma - i_{12}p)r_{b1}\right] u\omega_1 r_{b1}/i_{12} = 0 \end{aligned} \tag{12}$$

Equation (12) is the general expression of the contact line equation of the tooth surface.

3 Arc texture analysis of the tooth surface

3.1 Contact line analysis of tooth surface

In Eq. (12), the two variables u and θ should be determined, as well as the initial angle σ_0. The involute initial angle of the left tooth surface of the workpiece gear is σ_{01}, and the right initial

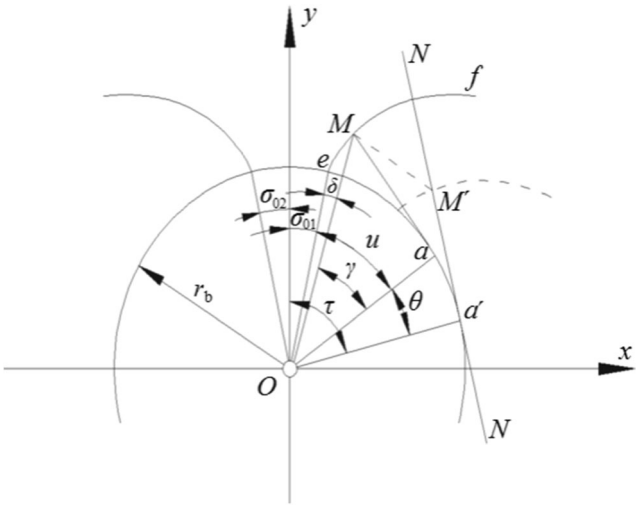

Fig. 3 The end-section parameters of the gear

angle is σ_{02}. The two initial angles are shown in Fig. 3. The *eM* angle of arbitrary point *M* on the involute *ef* is represented by δ, then these variables are expressed as:

$$\begin{cases} 0 \le \theta \le B_1/p \\ \sqrt{(r_{f1}/r_{b1})^2 - 1} \le u \le \sqrt{(r_{a1}/r_{b1})^2 - 1} \\ \delta = |u - \arctan u| \\ \sigma_{02} = \sigma_{01} + \pi/z_1 + 2\delta \end{cases} \tag{13}$$

where B_1 is the width of the workpiece gear, and r_{f1} and r_{a1} are the radius of the dedendum circle and addendum circle, respectively.

The relative parameters of workpiece gear and internal gear honing wheel are shown in Table 1.

According to the parameters listed in Table 1, the numerical solution of the nonlinear Eq. (12) can be obtained by using the MATLAB software and combining Eq. (13). Then the instantaneous contact line can be solved, as shown in Fig. 4, and more contact lines can be drawn on the tooth surface of the workpiece, as shown in Fig. 5.

As can be seen from Fig. 5, the changing process of the contact line from addendum to dedendum is short, long, and short. The changing process of the adjacent-instantaneous contact line is caused by the meshing motion, that is, the cutting trajectory is produced by the abrasive particles on the internal gear honing wheel from the instantaneous contact line of the workpiece tooth surface to the adjacent-instantaneous contact line. The cutting trajectory is the honed trajectory of the workpiece surface, which is related to the distribution of the cutting speed of the honed tooth surface. The relative velocity v_{WH}^{M} of arbitrary point *M* is superposed by the velocity v_d that along the tooth direction and the tooth profile velocity v_f, and the honing particles move at the cutting speed to form an arc honing trajectory, as shown in Fig. 6.

This is due to the staggered axis of honing wheel and workpiece, which makes the meshing point of honing gear produce relative slip velocity v_{WH}^{M} on the tooth surface, the density of arc texture depends on the size, and position of shaft angle Σ. Combined with the parameter data in Table 1, and rotation speed of internal gear honing wheel $n_H = 860$ r/min, according to the relative velocity of tooth contact line and contact trace discrete point in MATLAB, the tooth surface arc texture model is analyzed. After each instantaneous contact line is discretized, the distribution of relative velocity is simulated on the tooth surface of the workpiece, that is, the honed trajectory shown in Fig. 7.

In Fig. 7, arbitrary contact point is similar to an abrasive particle and is represented by a relative motion speed vector. If the honing trajectory of each abrasive particle is approximately connected, and then the reference circle is defined as the boundary (pitch circle when meshing), and the arc curve is presented with different angles toward the addendum and the dedendum. The texture of this typical arc trajectory is the feature of surface morphology, which is generated by the cutting of multi-particles on tooth surface during the process of power honing.

From the above analysis of shaft angle Σ, the changing of relative velocity is related to the changing of shaft angle Σ, which results in the changing of relative velocity of each contact point. The curvature of the arc trajectory is also changed. This arc trajectory is formed with the extension of the honing trajectory that induced by the cutting of multi-particles of the internal gear honing wheel. This can be seen in Fig. 8. The changing of the curvature can be seen from the changing of the Σ, that is, 0°, 5°, 10°, 15°, and 20°. Then the influence of

Table 1 The parameters of workpiece gear and internal gear honing wheel

Parameters of workpiece gear	Values	Parameters of internal gear honing wheel	Values	Units
Number of teeth z_1	73	Number of teeth z_2	123	/
Module m_{n1}	2.25	Module m_{n2}	2.25	mm
Pressure angle α_{n1}	17.5	Pressure angle α_{n2}	17.5	Degree
Spiral angle β_1	33	Spiral angle β_2	41.722	Degree
Modification coefficient x_1	0	Modification coefficient x_2	0	/
Width B_1	27	Width B_2	32	mm

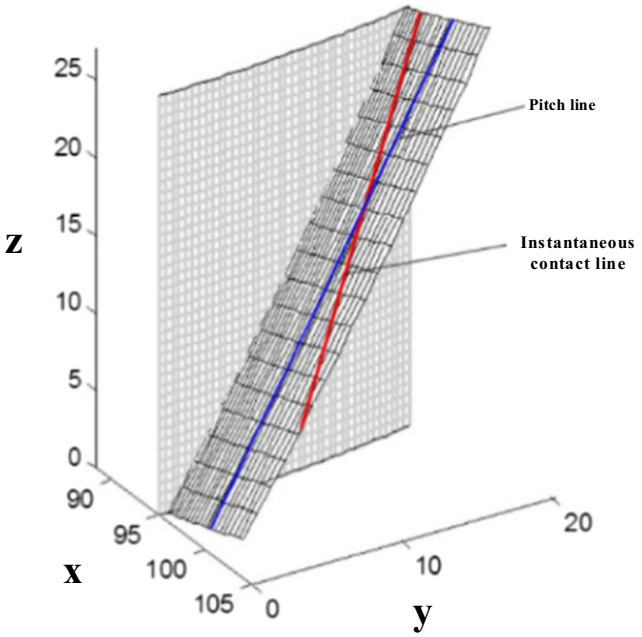

Fig. 4 The instantaneous contact line on the tooth surface of workpiece

the relative velocity of the tooth surface on the honing trajectory is further verified.

As can be seen from Fig. 8, when the value of shaft angle Σ is 0°, the honing trajectory is a straight line on the tooth profile and cannot form the arc trajectory, since the relative velocity of arbitrary contact points are along the tooth profile direction of workpiece tooth surface and there is no relative velocity in

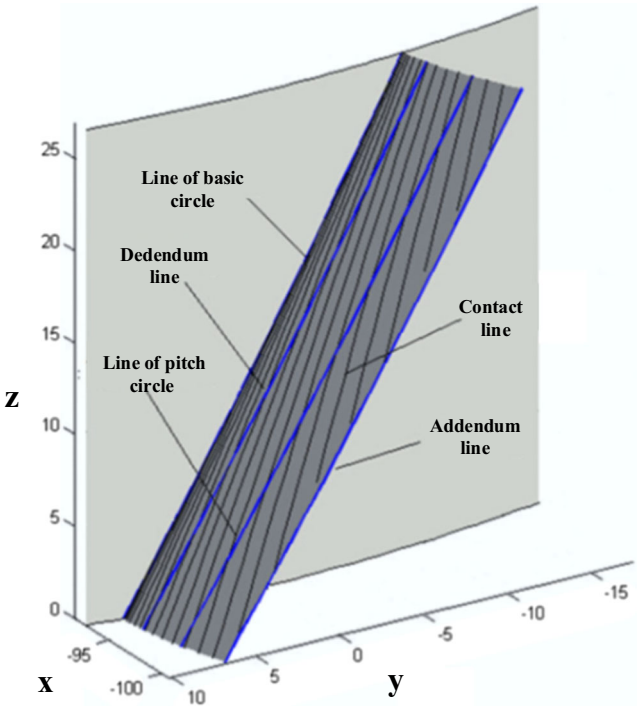

Fig. 5 The contact lines on the tooth surface of workpiece

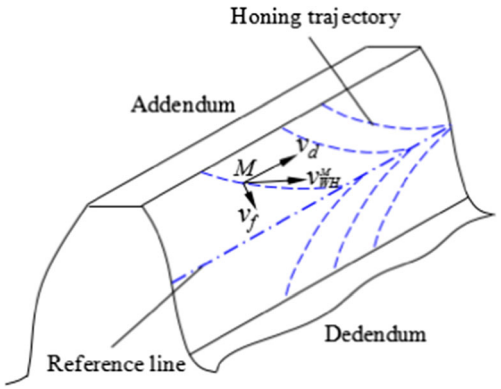

Fig. 6 Surface texture of gear honing

lead direction. In the actual gear honing process, if the feed of the axis direction of the workpiece is increasing, then the arc texture can also be generated on the workpiece tooth surface. When the shaft angle increases from 5° to 20°, the curvature of arc texture on the workpiece tooth surface will flatten and the radius of curvature increases at the same time. When the shaft angle is within the range of 10° to 15°, the arc texture is more obvious. When shaft angle decreases, the decreasing of relative velocity in tooth profile direction is less than that of lead direction. Therefore, the relative velocity of the tooth profile direction is a dominant one, while the relative velocity of the lead direction decreases until zero; therefore, the radius of arc curvature is small. When the shaft angle increases, the increasing range of the relative velocity in tooth profile direction is less than that of lead direction, which makes the large radius of arc curvature. Meanwhile, it is also shown that the relative velocity in lead direction of the reference circle is maximum,

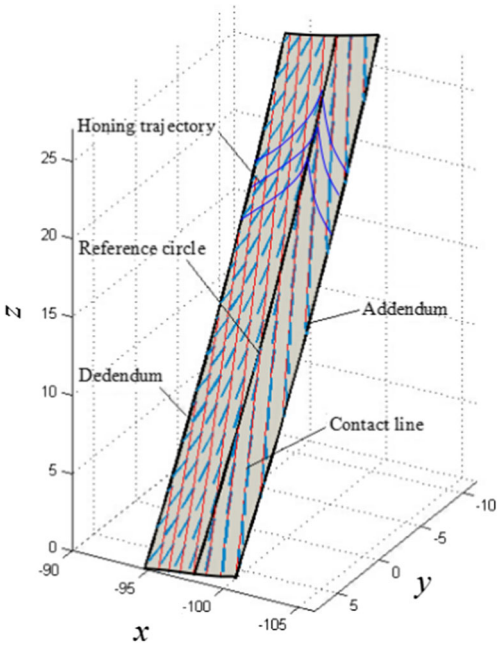

Fig. 7 The distribution of honed trajectory on tooth surface

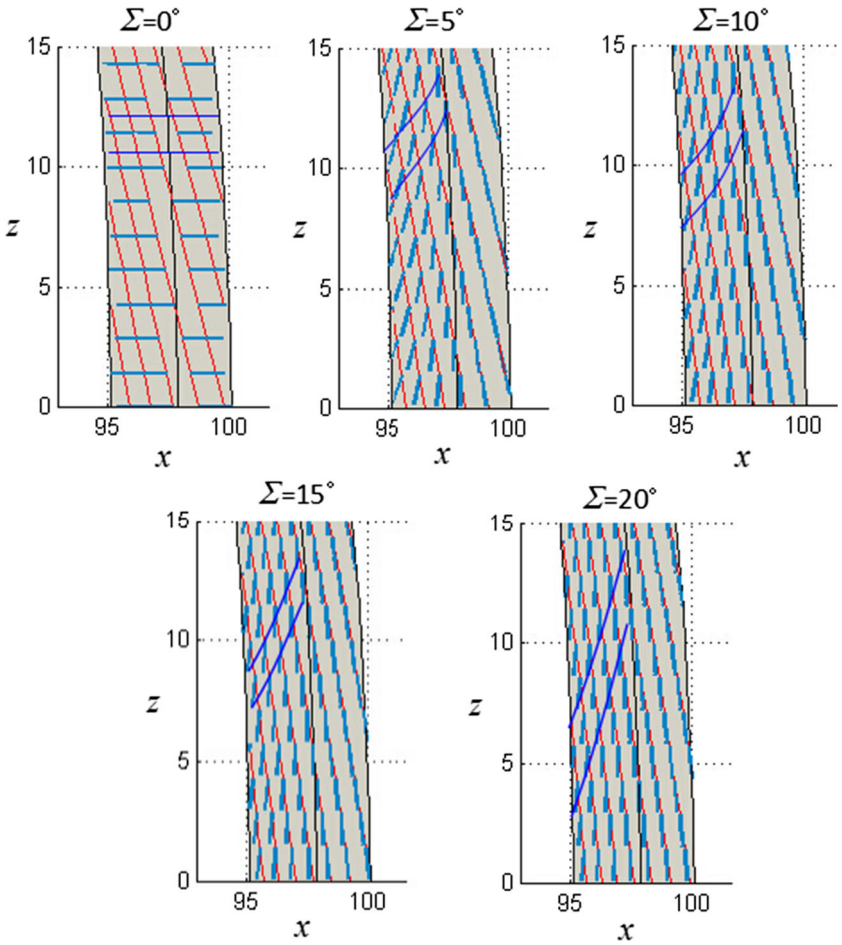

Fig. 8 The influence of shaft angle on honing trajectory

and then the phenomenon of multiple honing occurs in this nearby area during power honing moment. It is one of the main reasons for the "concave" phenomenon on the honed tooth surface.

Thus, in the actual honing process, reciprocating feed motion is required in the axis direction of the workpiece to make the whole workpiece tooth surface hone uniformly. So, it is advisable to choose the shaft angle within the range of 5° to 10°.

3.2 Experimental validation

In order to further understand the formation mechanism of surface arc texture of internal gear power honing, the internal honing wheel with ceramic AL_2O_3 material is used to power honing the workpiece gear with 20CrMnTiH material through four groups of process parameters (as shown in Table 2). Then the honed gear is detected and analyzed by imager and 3D profilometer, respectively. The imager is JVL250 and the objective is × 4.5 times. The geometric texture of the tooth surface is observed by the imager, and the honing texture near the reference circle is parallel to the lead direction. The dedendum and addendum are bending to the reference circle and presenting arc texture, as shown in Fig. 9.

In order to further compare the geometric texture of the tooth surface, the μsurf Expert 3D profilometer produced by NanoFocus Company of Germany is utilized, and the surface morphology of the first set of process parameters after honing was detected and analyzed. The type of this instrument is CLA01 with vertical and horizontal resolutions being 1.8 and 0.003 μm. The measured area of tooth surface is shown in Fig. 10. The tooth depth is 4.5 mm and the lead is 2.0 mm. The 3D profilometer is shown in Fig. 11 and the detection results are shown in Fig. 12.

According to the different testing methods, the results of Figs. 9 and 12 show that the texture of the tooth surface after gear honing is a kind of arc geometric texture and the theoretical analysis is verified.

Table 2 The parameters of honing process

Group	n_H (r/min)	f_Z (mm/min)	f_X (mm/min)
1	920	500	1×10^{-3}
2	920	300	1×10^{-3}
3	860	300	3×10^{-3}
4	1000	500	1×10^{-3}

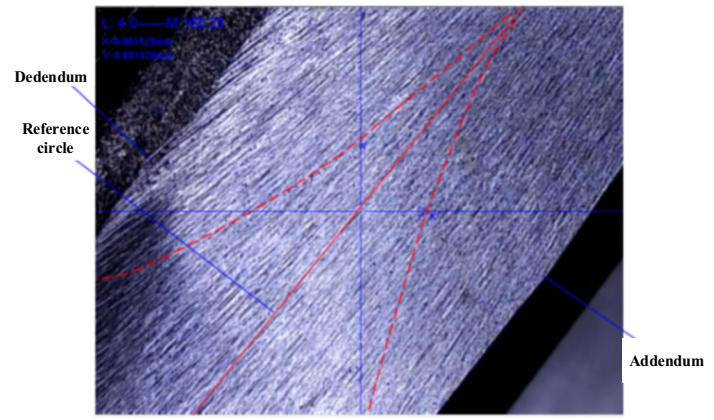

(a) The first group honing morphology

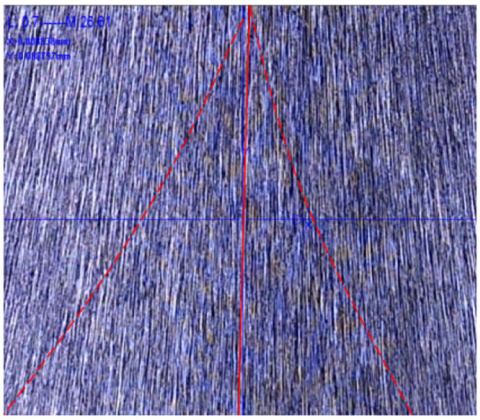

(c) The third group honing morphology

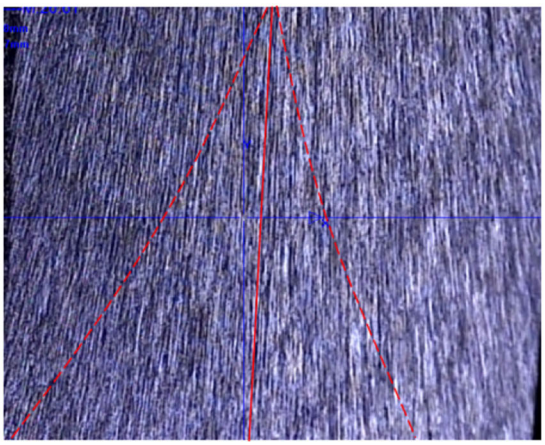

(b) The second group honing morphology

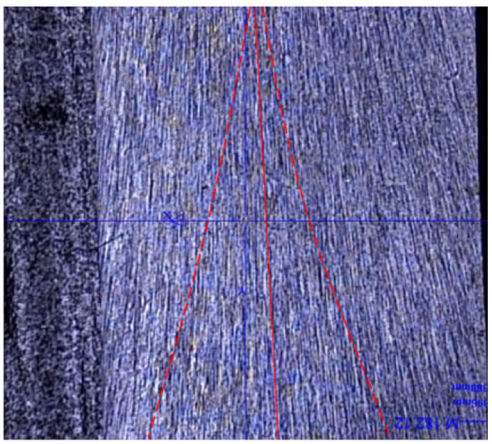

(d) The fourth group honing morphology

Fig. 9 Topography of tooth surface after honing. **a** The first group honing morphology. **b** The second group honing morphology. **c** The third group honing morphology. **d** The fourth group honing morphology

4 Regression modeling of tooth surface roughness

4.1 Modeling with response surface methodology

Response surface methodology (RSM) is a combination of mathematical method and statistical method. It is a statistical optimization method to solve multivariable problems and it is based on small sample test data [29]. This method investigates the relationship between input factors ($x_1, x_2, \ldots, x_n$) and output

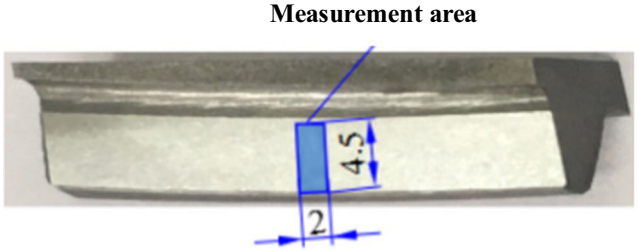

Fig. 10 The measured area of tooth surface

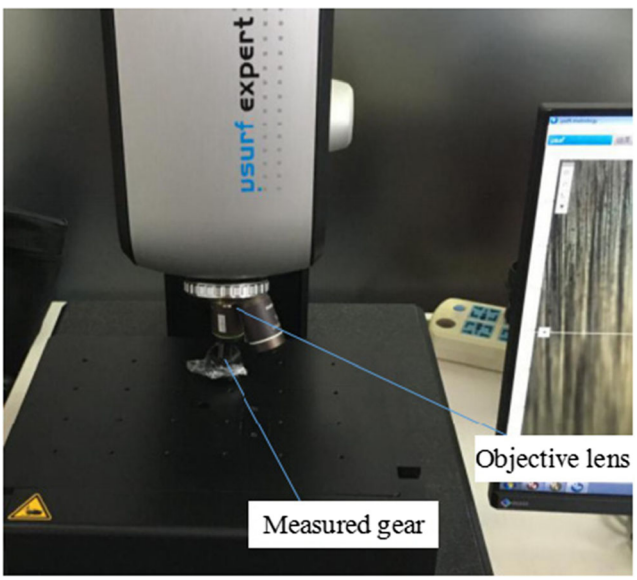

Fig. 11 The three-dimensional profilometer

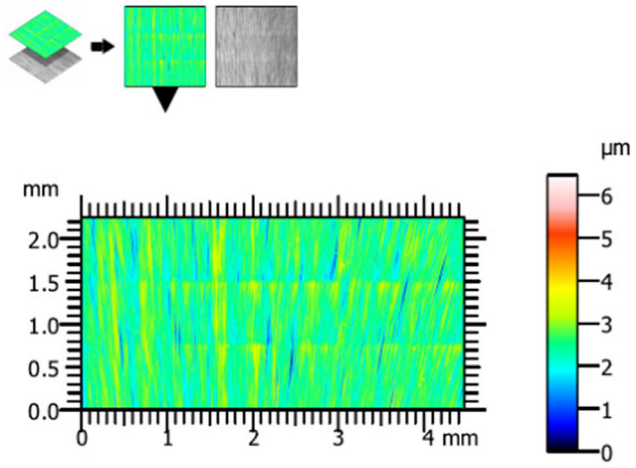

(a) Results of surface texture of two-dimensional detection

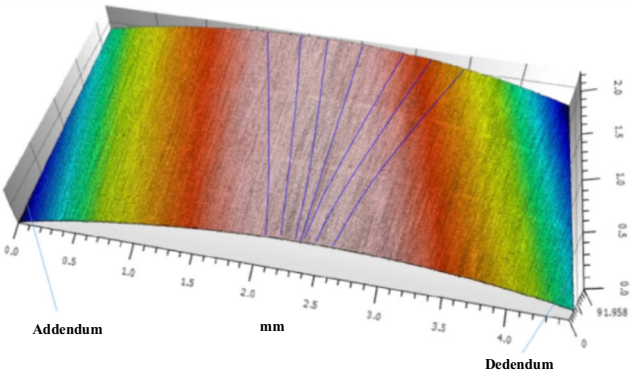

(b) Results of surface texture of three-dimensional detection

Fig. 12 Detection and analysis of surface texture. **a** Results of surface texture of two-dimensional detection. **b** Results of surface texture of three-dimensional detection

response $y(x)$. The process parameters of power honing are n_H, f_Z, f_X. The relationship between these three factors and output response R_a is a two-order response. The mathematical model is expressed as:

$$y(x) = b_0 + \sum_{i=1}^{n} b_i x_i + \sum_{i=1}^{n-1} \sum_{j=i+1}^{n} b_{ij} x_i x_j + \sum_{i=1}^{n} b_{ii} x_i^2 + \varepsilon \quad (14)$$

where b_{ij} is the interaction between x_i and x_j; b_{ii} is the quadratic effect of x_i.

The central composite face-centered (CCF) design method is applied in this paper. CCF designs the star point on its cube surface, and it has three levels, that is, 0,±1. Sometimes, the 0 level is not calculated, so the CCF design is also called the two levels, and its interaction term has the highest prediction accuracy. Meanwhile, it can guarantee the prediction accuracy of the first-term coefficient and the square term coefficient. CCF design is shown in Fig. 13.

According to Eq. (14), the quadratic response of surface equation is expressed as (15). This equation is the response of process parameters of internal gear power honing to surface roughness.

$$Y = R_a - \varepsilon = b_0 + \sum_{i=1}^{n} b_i x_i + \sum_{i=1}^{n-1} \sum_{j=i+1}^{n} b_{ij} x_i x_j + \sum_{i=1}^{n} b_{ii} x_i^2 \quad (15)$$

where R_a is surface roughness; Y is the prediction value of surface roughness; ε is the error term.

4.2 Experimental design

The Swiss-produced Fässler HMX-400 machine tool is utilized in the internal gear power honing test, this machine tool is shown in Fig. 14. The internal gear honing wheel is installed in the honing wheel rack and rotates in accordance with C_1 axis (the honing wheel speed is n_H), while the workpiece gear is installed at the end of the spindle head and it rotates in accordance with C_2 axis. The shaft angle between the internal tooth honing wheel and the workpiece gear can be adjusted by A axis. Z_1 and Z_2 feed axes, which can control the Z-direction feed F_Z of power honing gear. X axis can control X-direction feed f_X of the power honing gear. The cutting depth of the internal gear power honing is f_X and it changes in the actual cutting process. Therefore, the process parameters studied in this paper are based on the three process parameters applied in the actual production of the enterprise.

According to the actual production of enterprises and the range of Fässler provided process parameters of gear honing,

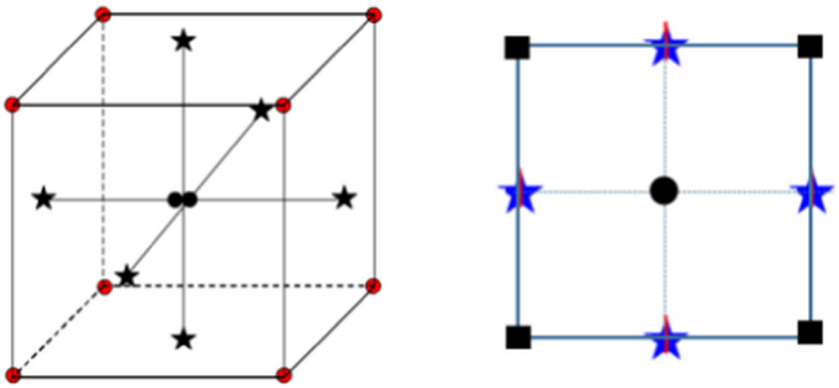

Fig. 13 Diagrammatic sketch of CCF

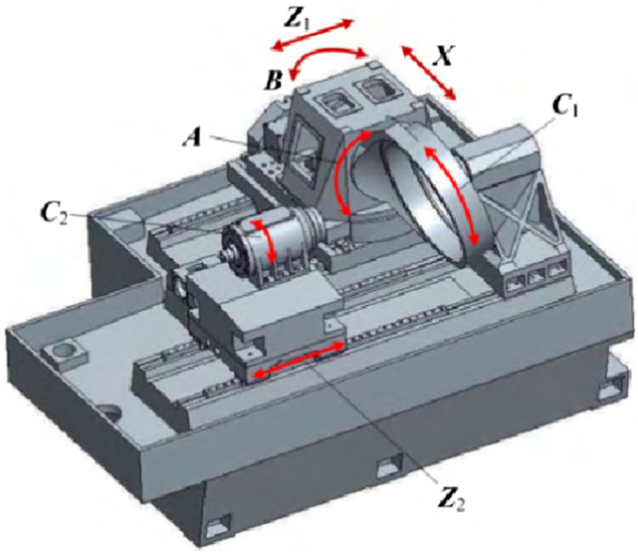

Fig. 14 Fässler HMX-400 machine tool

n_H is in the range of 720 to 1000 rpm, f_Z is in the range of 100 to 500 mm/min, and f_X is in the range of 1×10^{-3} to 5×10^{-3} mm/min. The relative gear parameters are shown in Table 1.

The experimental design point of CCF is based on Eq. (16).

$$N = 2^n + 2n + x_0 \tag{16}$$

where N is the test number; 2^n is the number of cube vertices under n factor; $2n$ is the number of stars in the direction of the cube along the axis; x_0 is the center point, and the value is 6.

n_H, f_Z, and f_X are the process parameters in the test. The influence factor n is 3, and the test number N is 20.

The test factor x_1 represents n_H, x_2 represents f_Z, and x_3 represents f_X. z_{-1}, z_0, and z_1 represent the −1,0 and 1 levels of process parameters, respectively. Then the three variables are encoded as:

$$\begin{cases} x_i = \dfrac{z_i - z_{0i}}{\Lambda_i}, i = 1,2,3 \\ \Lambda_i = \dfrac{z_{1i} - z_{0i}}{r} \end{cases} \tag{17}$$

where x_i are the encoding of variables; z_i are the variable parameters of honing process; z_{0i} is 0 level of the process variables of gear honing. Λ_i is variation range of the interval; r is 1 in CCF.

According to Eq. (17), the level of process parameters are encoded, which is shown in Table 3.

This experiment utilizes the Swiss produced portable surface roughness instrument TESA RUGOSURF 10, the resolution of the instrument is 0.01 μm/0.04 μm. The measurement of tooth surface for 20 gear parts after power honing is carried out. Since the tooth surface presents arc-shaped texture, the middle of the tooth width that nears the reference circle is measured. The measurement is along the tooth profile direction and combines the measuring features of stylus. As shown in Fig. 15, the arrow is the direction of the tooth surface with stylus measuring method, the detection results of specimen 1 are shown in Fig. 16.

Table 3 Coding table of factors level

Factors	Encoding	Level		
		−1	0	1
n_H	x_1	720	860	1000
f_Z	x_2	100	300	500
f_X	x_3	1×10^{-3}	3×10^{-3}	5×10^{-3}

4.3 Experimental modeling

As can be seen from Fig. 16, the detection result of gear specimen 1 is that $R_a = 0.669$ μm (The honing process parameters are that $n_H = 720$ rpm, $f_Z = 100$ mm/min, $f_Z = 5 \times 10^{-3}$ mm/min). In order to establish the response surface model of surface roughness, there are two analysis software for RSM, namely Design Expert and Minitab. In comparison, Design Expert is focus on experimental design, which can strike out an efficient test scheme and analyze the test data effectively. As a result, it can obtain a comprehensive and optimized results, as well as a visual model. In this CCF test, the Design Expert software of version 8.0 is employed.

Twenty test results are obtained after 20 times power honing. The test results are input to Table 4, then the corresponding surface equation of roughness is obtained through the analysis of Design Expert.

$$\begin{aligned} Y = {} & 0.61 - 0.19x_1 + 0.041x_2 + 0.026x_3 \\ & + 0.021x_1x_2 - 7.938 \times 10^{-3}x_1x_3 + 0.013x_2x_3 \\ & - 0.081x_1^2 - 0.024x_2^2 - 0.018x_3^2 \end{aligned} \tag{18}$$

where Y is theoretically predictive value of roughness. x_1, x_2, and x_3 are the encoding of process parameters with power honing.

4.4 Analysis of iso-surface

In order to accurately analyze the influence of honing parameters on roughness, the iso-surface graphs with different R_a

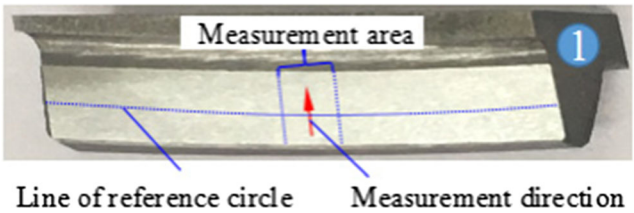

Fig. 15 The detection method of specimen 1

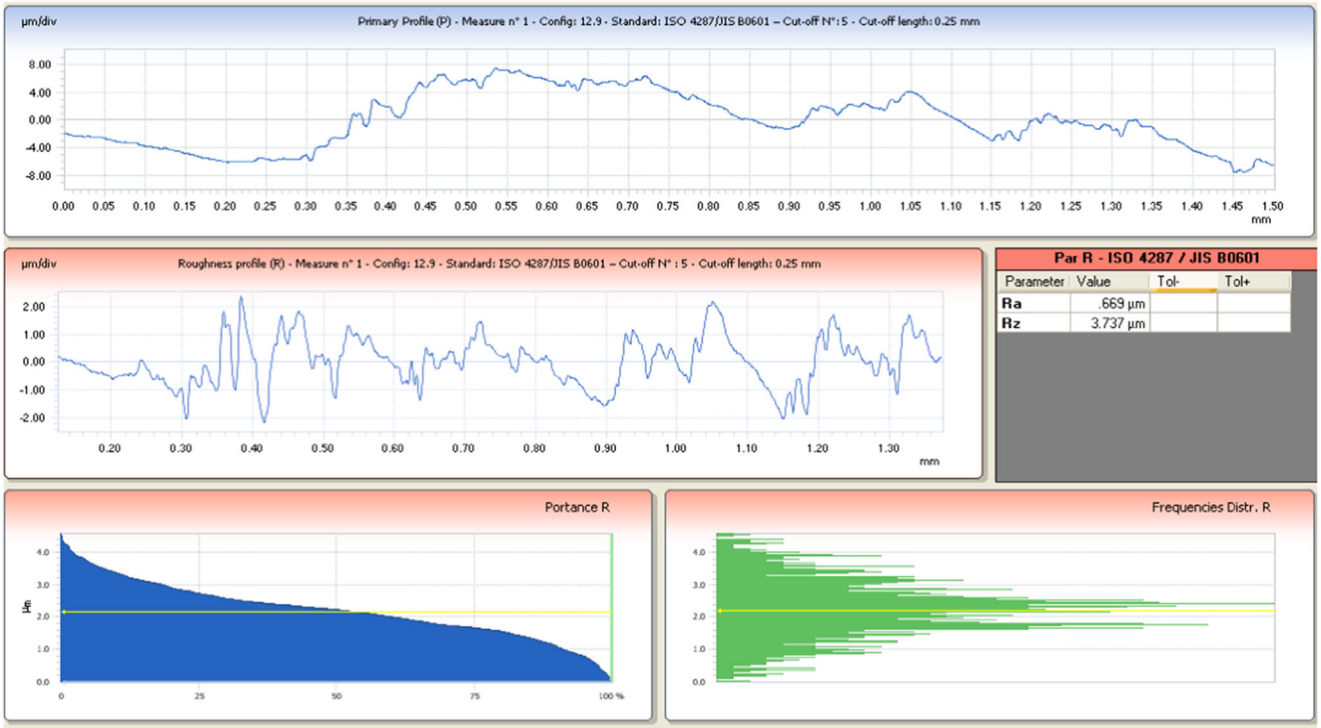

Fig. 16 The detection results of specimen 1

Table 4 List of the test data

S/N	n_H r/mim	f_Z mm/min	f_X µm/min	x_1	x_2	x_3	R_a µm
1	720	100	5	−1	−1	1	0.669
2	860	300	3	0	0	0	0.601
3	720	500	1	−1	1	−1	0.651
4	860	500	3	0	1	0	0.612
5	1000	500	5	1	1	1	0.434
6	1000	300	3	1	0	0	0.368
7	860	100	3	0	−1	0	0.567
8	720	500	5	−1	1	1	0.756
9	860	300	3	0	0	0	0.600
10	720	300	3	−1	0	0	0.697
11	860	300	5	0	0	1	0.621
12	1000	100	5	1	−1	1	0.233
13	860	300	1	0	0	−1	0.570
14	720	100	1	−1	−1	−1	0.639
15	1000	100	1	1	−1	−1	0.212
16	720	300	3	−1	0	0	0.697
17	860	300	5	0	0	1	0.620
18	1000	500	1	1	1	−1	0.331
19	860	300	3	0	0	0	0.599
20	1000	100	5	1	-1	1	0.233

values for Eq. (18) are plotted by means of MATLAB. R_a is 0.3, 0.4, 0.5 and 0.6 µm, respectively. The four iso-surface graphs are shown in Fig. 17.

As can be seen from Fig. 17a, x_1 is in the range of 0.8 to 1. In Fig. 17b, x_1 is in the range of 0.4 to 1. In Fig. 17c, x_1 is in the range of 0 to 0.8. In Fig. 17d, x_1 is in the range of − 0.6 to 0.4. Thus, with the increase of R_a, the value of the influence factor x_1 is close to the low level. x_1 has a minimum range of value, no matter what the R_a value is. Therefore, the influence factor x_1 has the greatest effect on R_a value. When R_a decreases from 0.4 to 0.3 µm, the range of the influence factor x_2 has a little reduction while x_3 is almost not change, which can be seen from Fig. 17a, b. It can be seen that the influence effect of x_2 on R_a value is slightly higher than that of x_3. That is, when $R_a \geq 0.4$ µm, the influence of x_2 and x_3 are almost the same, when $R_a \leq 0.3$ µm, the influence of x_2 is slightly higher than that of x_3. The analysis results show that n_H has the greatest influence on the surface roughness of the workpiece gear. When $R_a \geq 0.4$ µm, the influence of f_Z and f_X is almost the same, when $R_a \leq 0.3$ µm, the influence of f_Z is slightly higher than f_X.

5 Model verification

Considering the error of instrumental measurement and in order to verify the accuracy of the regression model, a group of 20 measurement results shown in Table 5 were obtained by

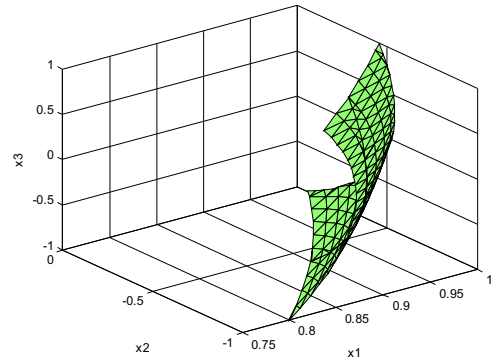

(a) An iso-surface graph with R_a=0.3μm.

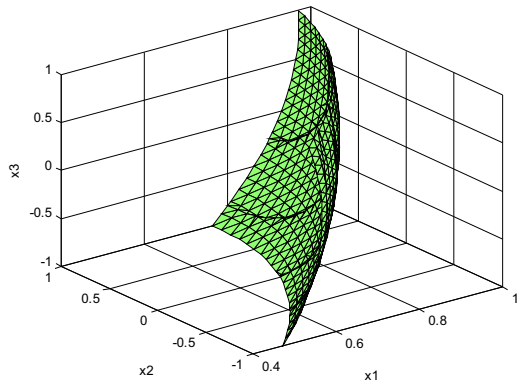

(b) An iso-surface graph with R_a=0.4μm.

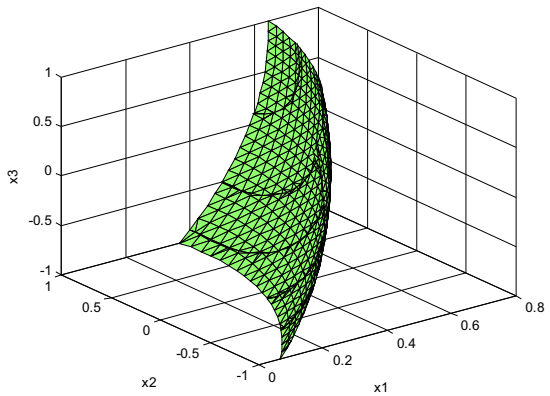

(c) An iso-surface graph with R_a=0.5μm.

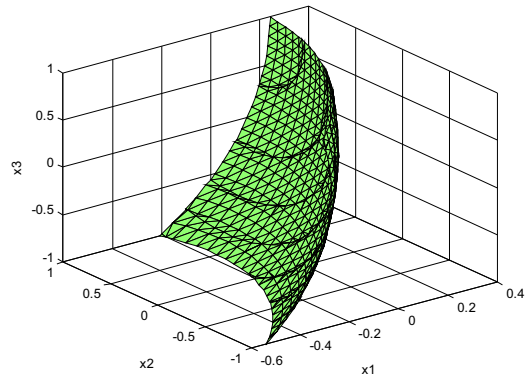

(d) An iso-surface graph with R_a=0.6μm.

◀ **Fig. 17** The equivalent surface graphs of different R_a values. **a** An iso-surface graph with $Ra = 0.3$ μm. **b** An iso-surface graph with $Ra = 0.4$ μm. **c** An iso-surface graph with $Ra = 0.5$ μm. **d** An iso-surface graph with $Ra = 0.6$ μm

means of non-contact profilometer. The measured value 1 is the result of contact needle measurement, 2 is the result of non-contact profilometer, and the regression value is calculated by regression equation. The accuracy of the test results can be calculated by formula (19). The average error of the final test results is 4.52%, while it is 3.06% for the calibration results of the contactless profilometer. It can be seen that the surface roughness model established by the response surface method has a high setting degree and good predictive control effect.

$$\begin{cases} \Delta_i = \left| \dfrac{Y_{\text{exp}i} - Y_{\text{theo}i}}{Y_{\text{exp}i}} \right| \times 100\% \\ \Delta = \dfrac{\sum_{i=1}^{N} \Delta_i}{N} \end{cases} \tag{19}$$

where Δ_i is the error value of the ordinal point i, Y_{expi} is the test value of ordinal point i, Y_{theoi} is the regression theory value of ordinal point i, Δ is the average error of this regression model, N is the number of points in this test, and $N = 20$.

Table 5 Comparison of two kinds of measurement results with regression theory value

S/N	Measured value 1	Measured value 2	Regression value
1	0.669	0.677	0.678
2	0.601	0.609	0.61
3	0.651	0.652	0.65
4	0.612	0.622	0.627
5	0.434	0.423	0.39
6	0.368	0.359	0.339
7	0.567	0.551	0.545
8	0.756	0.757	0.744
9	0.6	0.599	0.61
10	0.697	0.685	0.719
11	0.621	0.616	0.618
12	0.233	0.236	0.24
13	0.57	0.56	0.566
14	0.639	0.629	0.636
15	0.212	0.222	0.299
16	0.697	0.71	0.719
17	0.62	0.621	0.618
18	0.331	0.332	0.328
19	0.599	0.612	0.61
20	0.233	0.237	0.24

6 Conclusions

According to the theoretical and experimental analysis, it is proved that the NC internal gear power honing can generate arc texture on the surface of the honed gear, and the generated arc geometric texture is suitable when Σ is in the range of 5° to 10°. It is also showed that n_H has the greatest influence on the surface roughness of the workpiece gear. When $R_a \geq 0.4$ μm, the influence of f_Z and f_X is almost the same, when $R_a \leq 0.3$ μm, the influence of f_Z is slightly higher than f_X. The results are applied to predict and control the surface quality of the workpiece gear before honing.

Funding information This study is mainly funded by the National Natural Science Foundation of China (Grant No.51575154), and the Major National R&D Projects (Grant No.2013ZX 04002051).

References

1. Hu DH, Zhang L, Guo GL, Wang PJ (2016) Tool presetting method for grinding based on the worst angles of tooth space edges. Int J Adv Manuf Technol 82(5):921–926
2. Aloso U, Ortega N, Sanchez JA, Pombo I, Plaza S, Izquierdo B (2014) In-process prediction of the hardened layer in cylindrical traverse grind-hardening. Int J Adv Manuf Technol 71(1):101–108
3. Hu YJ, Wang YQ, Zhao GL, Wang Y, Yuan XH (2011) Feature-based modeling of automobile gears and maufactureing resources for virtual manufacturing. Int J Adv Manuf Technol 55(1):405–419
4. Brecher C, Brumm M, Hübner F (2015) Approach for the calculation of cutting forces in generating gear grinding. Procedia CIRP 33:287–292
5. Sandro PS, Lincoln CB, Luis HG, de Zelda CS (2012) Finishing process analysis between honing and hard hobbing in pinion gears applied to a steering system. Energy Procedia 14(2012):2–8
6. Silva SP, Brandao LC, Rafael FPP (2011) Evaluation of quality of steering systems using the honing process and surface response methodology. Adv Mater Res 223:821–825
7. Bouzakis KD (2008) Manufacturing of cylindrical gears by generating cutting processes: A critical synthesis of analysis methods. CIRP Annals 57(2):676–696
8. L.C Brandão, S P Silva, GA Abreu, PC Lima (2009) O processo de acabamento em pinhões de sistemas de direção. In: COBEF-Congresso Brasileiro de Engenharia de Fabricação. pp 11–20
9. Amini N, Westberg H, Klocke F (1999) An experimental study on the effect of power honing on gear surface topography. Gear Technol 16(1):11–18
10. Jolivet S, Mezghani S, Issenlin J, Mansori EI (2016) Numerical simulation of tooth surface finish effects on gear noise. Appl Scien Technol Sour 102:436–443
11. Jolivet S, Mezghani S, Mansori EM, Jourdain B (2015) Dependence of tooth flank finishing on powertrain gear noise. J Manuf Syst 37(42):467–471
12. Denkena B, Schindler A, Woiwode S (2016) Calculation method of the contact area in flank machining for continuous generating grinding. Appl Math Model 40(15–16):7138–7146
13. Chakrabarti S, Paul S (2008) Numerical modeling of surface topography in super-abrasive grinding. Int J Adv Manuf Technol 39(1): 29–38
14. Nguyen TA, Butler DL (2005) Simulation of precision grinding process, Part1: generation of the grinding wheel surface. Int J Mach Tools Manuf 45(11):1321–1328
15. Hecker RL, Liang SY (2003) Predictive modeling of surface roughness in grinding. Int J Mach Tools Manuf 43(8):755–761
16. Stepien P (2009) A probabilistic model of the grinding process. Appl Math Model 33(10):3863–3884
17. Thyssen W (2006) Erfahrungen und visionen mit der CNC-Hochleistungs-Schleifmaschine RZ 150/RZ 400 HEUTE und in ZUKUNFT, Presentation Company Reishauer, Wallisellen. (CH)
18. Karpuschewski B, Knoche HJ, Hipke M (2008) Gear finishing by abrasive process. CIRP Ann Manuf Technol 57:620–640
19. Chen ST, Hu HF, Zhang C (2015) Surface roughness modeling based on laser speckle imaging. Acta Phys Sin 64(23):234203
20. Ho WH, Tsai JT, Lin BT, Zhou JH (2009) Adaptive network based fuzzy inference system for prediction of surface roughness in end milling process using hybrid Taguchi-genetic learning algorithm. Expert Syst Appl 36(2):3216–3222
21. Thomas TR (1982) Rough surface. Longman, London
22. Whitehouse DJ (1994) Handbook of surface metrology. Bristol, UK: Institute of Physics
23. Tsai YS, Chen JC, Lou SJ (1999) An in-process surface recognition system based on neural networks in end milling cutting operations. Int J Mach Tools Manuf 39(4):583–605
24. Suykens JAK, Vandewalle J (1999) Least squares support vector machine classifiers. Neural Process Lett 9(3):293–300
25. Caydas U, Ekici S (2012) Support vector machines models for surface roughness prediction in CNC turning of AISI 304 austenitic stainless steel. J Intell Manuf 23(3):639–650
26. Sandro S, Moni RF, Lincoln CB (2014) Particle swarm optimization for achieving the minimum profile error in honing process. Pre Eng J Int Societ Pre Eng Nanotechnol 38(4):759–768
27. Sayles RS, Thomas TR (1978) Surfaces topography as a non- stationary random process. Nature 27(1):431–434
28. Litvin FL, Fuentes A (2004) Gear geometry and applied theory, second edn. Cambridge University Press, New York
29. Thirugnanasambandham K, Sivakumar V (2015) Optimization of treatment of grey wastewater using electroFenton technique-modeling and validation. Process Saf Environ Prot 95:60–68